A 3-D Computational Model for Multicellular Tissue Growth

Lenny Tang and Belgacem Ben Youssef

School of Interactive Arts and Technology
Simon Fraser University
Surrey, British Columbia, V3T 5X3, Canada
{lctang, byoussef}@sfu.ca

Abstract. We report the development of a computational model for the growth of multicellular tissues using a discrete approach based on cellular automata to study the tissue growth rates and population dynamics of two different populations of migrating and proliferating mammalian cells. Cell migration is modeled using a discrete-time Markov chain approach and each population of cells has its own division and motion characteristics that are based on experimental data. A large number of parameters allow for a detailed study of the population dynamics. This permits the exploration of the relative influence of various system parameters on the proliferation rate and some other aspects of cell behavior such as average speed of locomotion.

1 Introduction

A primary goal of tissue engineering is to create three-dimensional tissues with the proper structure and function. Natural tissues are multicellular and have a specific three-dimensional architecture. This structure is supported by the extracellular matrix (ECM). The ECM often has the form of a three-dimensional network of cross-linked protein strands. In addition to determining the mechanical properties of a tissue, the ECM plays many important roles in tissue development. Biochemical and biophysical signals from the ECM modulate fundamental cellular activities, including adhesion, migration, proliferation, differentiation, and programmed cell death [1].

Scaffold properties, cell activities like adhesion or migration, and external stimuli that modulate cellular functions are among the many factors that affect the growth rate of tissues. Hence, the development of bio-artificial tissue substitutes involves extensive and time-consuming experimentation. The availability of computational models with predictive abilities will greatly speed up progress in this area. This research focuses on the development of a model to simulate the growth of three-dimensional tissues consisting of more than one cell type. Specifically, this model can be used to study how the overall tissue growth rate is affected by:

- cell migration speed;
- the initial density of the seed cells; and
- their spatial distribution.

M. Harders and G. Székely (Eds.): ISBMS 2006, LNCS 4072, pp. 29–39, 2006.

The rest of the paper is organized as follows: Section 2 describes some of the earlier work. Section 3 introduces the concepts of cellular automata. Section 4 discusses the modelling of the biological system. In Section 5, we discuss the sequential simulation results. We conclude the paper in Section 6.

2 Previous Work

Earlier studies by other investigators developed cellular automata models for 2-D problems involving aggregation and self-organization of the cellular slime mold *Dictyostelium Discoideum* or interactions between extracellular matrix and fibroblasts ([2], [3], and [4]). In addition, some of the previous research involved the development of computational models that are deterministic or stochastic in nature ([5] and [6], respectively).

Ben Youssef developed a computational model for tissue growth in three-dimensional scaffolds using a single type of mammalian cells [7]. Our work presented here builds on this 3-D model by extending its functionality to incorporate a variable number of cell types. The objective is to build theoretical models and computer simulation tools for tissue engineering [8].

3 Cellular Automata

Cellular automata (CA) were originally introduced by John von Neumann and Stan Ulam as a possible idealization of biological systems with a particular purpose of modeling biological self-reproduction [9]. This approach has been used since then to study a wide variety of physical, chemical, biological, and other complex natural systems.

The use of cellular automata in modeling various systems including biological ones has some advantages that include providing a computationally proficient technique for analyzing the collective properties of a network of interconnected cells as well as an alternative approach involving discrete coordinates and variables to represent the complex dynamic system where the model behaviour is completely specified by a simple operating mechanism in terms of local relations. This may be sufficient to support a whole hierarchy of structures and phenomena.

4 Model Development

The growth of tissue is a complex biological process. The migration and proliferation of mammalian cells is characterized by the following three subprocesses: cell division, cell motion, and cell collision. Due to space limitations, we will omit discussing the steps involved in modeling these subprocesses. The reader is referred to [7] and [10] for related descriptions.

4.1 States of Cellular Automata

The cellular space is comprised of N_t=$N_x \times N_y \times N_z$ computational sites. The automata in this space are governed by the von Neumann's neighborhood in three dimensions.

That is, the 6 neighbors of a cell c are to its east, north, west, south, and directly above and below it. Each occupied computational site in the model must describe the current state of a given cell. According to our modeling steps above, the requisite state information is as follows:

1. The type of cell.
2. The direction of cell motion.
3. The speed of the cell.
4. The remaining time until a change of direction.
5. The remaining time until the next cell division.

Hence, the state of a cell can be defined as a single eight-digit number in the following way:

$$\Upsilon = \{jklmnpqr | j, k, l, m, n, p, q, \text{and } r \in \mathbb{N}\},$$

where *j* identifies the cell type. The direction of motion is designated by *k*. When *k* is 0, the cell is in a stationary state. When the value ranges from $1 - 6$, it denotes one of the six directions in which the cell is currently moving. The digits lm identify the time until the next change in direction, called the *persistence counter*. The *cell phase counter* is denoted by $npqr$. The cell phase counter is the time remaining until the cell is ready to divide.

4.2 Mixed Cell Cultures and Tissue Architecture

Most tissues consist of several types of cells that organize themselves in very specific spatial patterns [11]. This three-dimensional architecture is what endows tissues with the special functions of organs. While previous studies have focused on a single type of cells, our model allows for simulating multiple cell types, with each cell type having its own migratory and proliferation characteristics. The model allows for the organization of cell populations into specific spatial patterns. Tissue engineers are attempting to achieve this goal by using microlithographic techniques to create surfaces with heterogeneous characteristics and solids with specific pore structure. When micro-patterned surfaces are used, different cells will migrate at different rates on different parts of the surface. Thus, we can guide cells of certain type to cluster in specified areas only. These areas may be surrounded by cells of another type.

5 Simulation Results and Discussion

5.1 Initial Conditions and Model Parameters

The simulations of the proliferation of multiple cell types are obtained using a $100 \times 100 \times 100$ cellular array where two cell populations are used. Cells of population 1 are faster moving cells while cells of population 2 are slower moving cells. We define R as the ratio of the initially seeded number of cells from these two cell populations. This is given by

$$R = \frac{\text{initial number of cells from population 1}}{\text{initial number of cells from population 2}}.$$

That is, when $R = 9$, there are 9 cells from population 1 for every cell from population 2.

We consider two seeding topologies: a uniform topology and a "wound healing" topology. In the former, the cells are randomly seeded in the cubic space. In the latter, an empty cylinder is surrounded by seeded cells in the remainder of the cellular space. The empty cylinder has a diameter of 50 and a height of 100. In addition, for each topology, we consider two seeding distributions:

1. *Mixed distribution*: The different cell types are seeded together according to the used cell distribution.
2. *Segmented distribution*: Each cell type is seeded in a separate area of the cellular space.

The migration speeds of cells in populations 1 and 2 are equal to 10 μm per hour and 1 μm per hour, respectively. Throughout these simulations, a confluence parameter of 100% and an average waiting time of 2 hours for the six directions of motion are utilized. Each cell is modeled as a cubic computational element whose sides are equal to 10 μm. We also use different division distributions for these two cell populations. The division times are given in Table 1.

Table 1. Division Time Distribution for the Two Cell Populations

	Cell Populations	
Division Times	Cell Population 1	Cell Population 2
12 - 18 hrs	64%	4%
18 - 24 hrs	32%	32%
24 - 30 hrs	4%	64%

The flexibility of the model permits the exploration of the influence of several system parameters on the growth rate and some other aspects of cell behavior such as the average cell speed. For instance, to compute the overall tissue growth rate, we use the following formula:

$$\frac{dk(t)}{dt} = \frac{\sum_{i=1}^{n} N_{c_i}(t) - N_{c_i}(t - \Delta t)}{\Delta t \times N_t},$$

where $k(t)$ is the cell volume fraction at time t as given in [12], Δt is the time step in days, N_t is the size of the cellular space (=$N_x \times N_y \times N_z$), $N_{c_i}(t)$ is the number of occupied computational sites by cell type i at time t, and n is the number of cell types ($n \geq 1$).

5.2 Uniform Topology

Effect of Seeding Density. Figure 1 shows the effect of the seeding density on the tissue growth rate. Here, cells from both populations are seeded in a mixed pattern using

a uniform distribution. The seeding density of population 2 is held constant at 0.1% while the seeding density of population 1 is varied from 0.1% to 10%. As expected, the time required to reach confluence decreases with the increase of the initial seeding density. We see that when the initial seeding density of population 1 is greater than 1%, the impact of cell division can be readily observed by the plateaus formed on the corresponding growth rate curves. The division time distributions of population 1 and population 2 specify that respectively 64% and 4% of cells will divide between 12-18 hours. This is depicted by the first plateau on the indicated curves for seeding densities of 5% and 10%. Additional plateaus are observed at later times reflecting the succeeding waves of cell divisions during the proliferation process. The subsequent waves of cell divisions include not only seeded cells giving birth to new cells but also daughter cells going through their own mitotic cycles. For small seeding densities, the growth rate curves show a more gradual increase that indicates a lower, though steady, overall impact on the tissue growth rate.

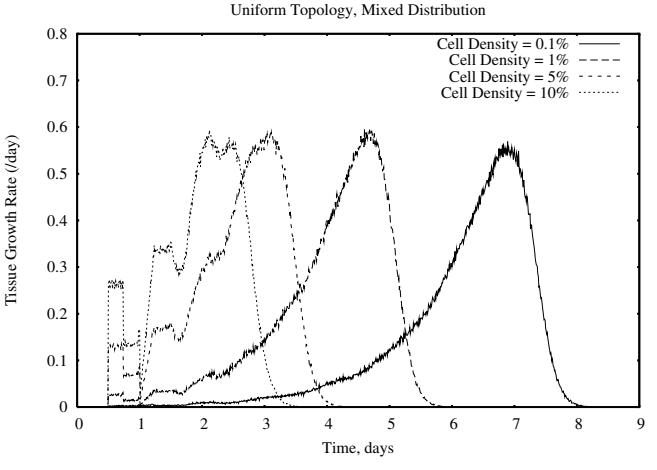

Fig. 1. Effects of varying the seeding density on the overall tissue growth rate. The seeding density of population 2 (slow-moving cells) is held constant at 0.1% while the seeding densities of fast-moving cells are varied.

Effect of Cell Heterogeneity. Figure 2(a) shows the tissue growth rate versus time for different values of the ratio R. In these simulation runs, R is equal to 1, 3, 5, and 9 while the total initial seeding density is maintained at 0.5%. For instance, with $R = 9$ the faster moving population of cells covers 90% of the cellular space while the slower moving population covers the remaining 10%. We observe that as R increases, the time taken to reach confluence decreases. This is because for larger values of R, the population of faster moving cells dominates the proliferation. This is clearly depicted in this figure where a higher tissue growth rate is observed as R is increased. Faster moving cells spread out in the cellular space preventing the formation of cell colonies; thus allowing for confluence to be reached sooner.

The effects of varying R on the tissue growth rate in a mixed distribution was also studied and is shown in Fig. 2(b). In these simulations, the total seeding density is 0.5%. We observe similar results to the ones obtained when using a segmented distribution. However, when $R = 1$, the mixed distribution yields a higher tissue growth rate (compare Fig. 2(a) with Fig. 2(b)). This may be attributed to the fact that contact inhibition has less of an effect in the mixed distribution where faster cells have more nearby empty spaces to move into, which in turn frees up sites for the slower-moving cells.

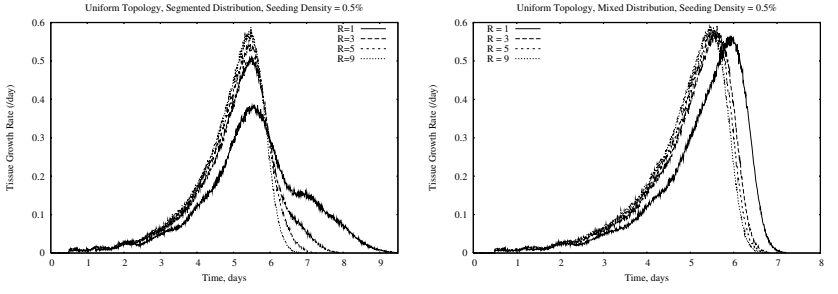

(a) (b)

Fig. 2. Overall tissue growth rate versus time for various values of ratio R in the case of two cell-seeding distributions

Effect of Cell-Seeding Distributions. Figure 3 show a comparison between the tissue growth rates obtained by using the segmented and mixed distributions of the uniform cell-seeding topology. Here, $R = 1$ and a seeding density of 0.1% are used. Cells from population 2 migrate at a fixed speed of 1 μm/hr. In both these figures, cells from population 1 have a migration speed of 10 μm/hr in part (a) and 50 μm/hr in part (b), respectively. We observe that the mixed-seeding distribution takes less time to reach confluence and yields higher tissue growth rates. However, as cell speeds increase, the difference between both seeding modes diminishes. Higher cell motility allows cells in the segmented distribution to move far away from their original seeded sites and disperse in the cellular space to minimize the impact of contact inhibition, thus creating a transient distribution that resembles the one induced by the mixed distribution. Moreover, with mixed seeding, the effects of increasing cell speed are less pronounced. For instance, the tissue growth rate curves are nearly identical for both population 1 speeds when a mixed distribution is used as in both cases confluence is reached in about 8 days and their growth rate curves are very similar. Increasing population 1 speeds is more beneficial in the case of a segmented distribution where an enhanced tissue growth rate and a reduction in the time to reach confluence are both observed.

5.3 Wound-Seeding Topology

Effect of Cell Speed. The growth rate curves in Fig. 4(a) and (b) demonstrate the effect of motility on volume coverage in the case of a wound-seeding mode using both

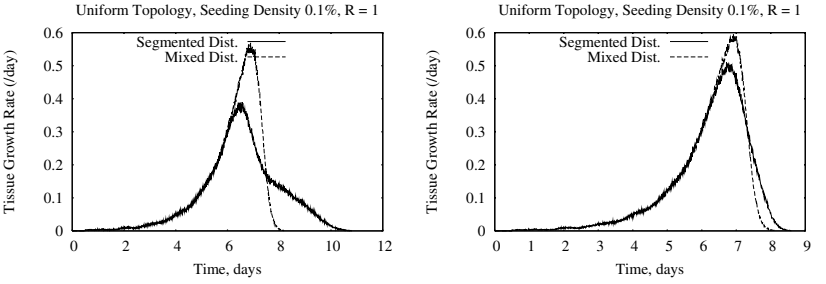

Fig. 3. Comparison of tissue growth rate for two cell-seeding distributions. Here, the migration speed of cells from population 2 is maintained at 1 μm/hr while cells from population 1 move at speeds of 10 μm/hr (part (a)) and 50 μm/hr (part (b)), respectively.

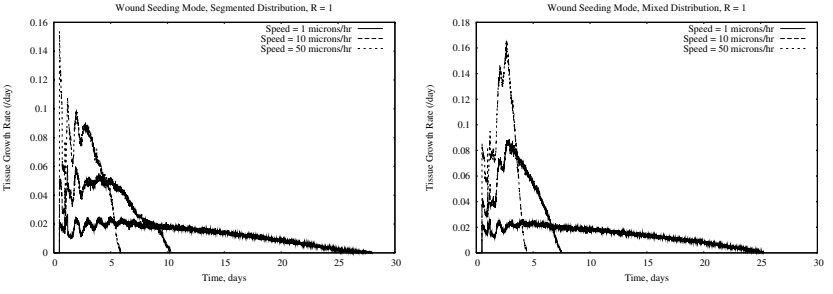

Fig. 4. Effect of varying the cell speed of population 1 on the overall tissue growth rate. Cells in population 2 move at a fixed speed of 1 μm/hr.

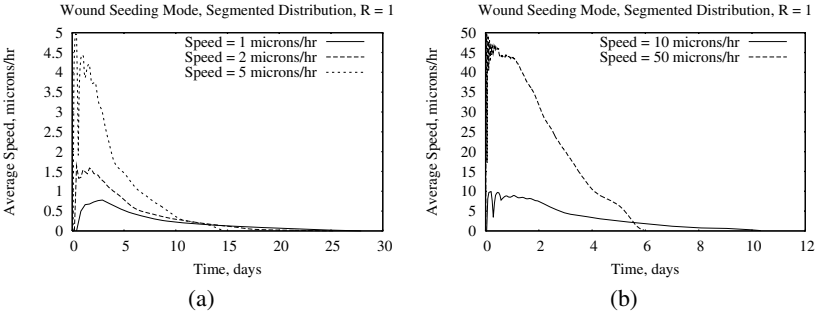

Fig. 5. The effect of cell motility (population 1) on the population-average speed of locomotion for cell speeds ranging from (a) 1 to 5 μm/hr and (b) 10 to 50 μm/hr

a segmented and mixed distribution with $R = 1$, respectively. We observe that as the motility of the cell increases, the tissue growth rate increases and confluence is attained faster; thus, healing the wound. Higher motility of cells decreases the impact of contact

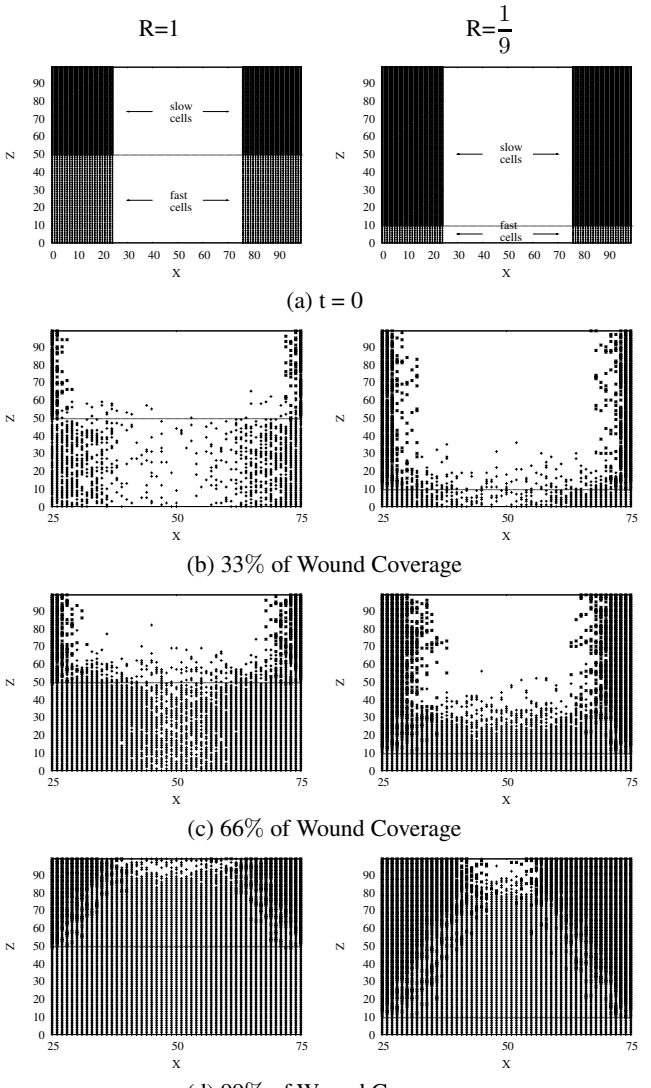

Fig. 6. Cell population profiles shown as 2-D cross sections of two simulation runs at t = 0 and at 33%, 66% and 99% of wound coverage for $R = 1$ and $R = \frac{1}{9}$, respectively. For illustration purposes, we included a horizontal line to distinguish between the two cell-seeding populations.

inhibition on the proliferation rate as it reduces the formation of cell colonies. Moreover, the tissue growth rate is the highest when cells in population 1 move at the fastest speed of 50 μm/hr. Highly motile cells cover the wound area faster, thus allowing them to reach far away, empty sites quickly and affording them additional opportunities for division. Figure 5 depicts the population-average speed in the denuded area (that is, the initially empty cylinder) for different speeds of population 1. At the beginning of the

simulations, cells move into the "wound" at their peak speeds. The overall cell speeds drop rapidly as the "wound" becomes congested with new daughter cells and collisions become more frequent. The average speed decreases with time and shows a drastic decrease as confluence is attained due to the formation of local clusters.

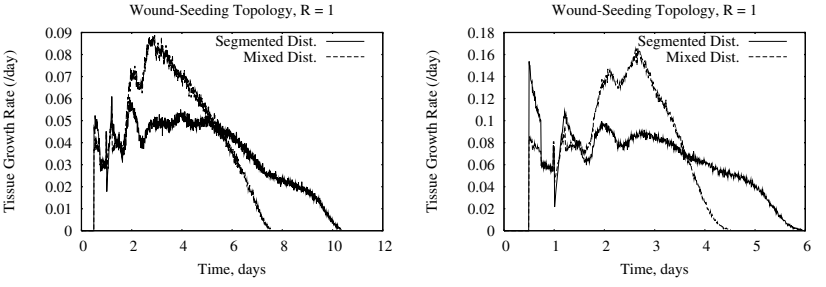

Fig. 7. Comparison of tissue growth rate for two cell-seeding distributions. In both seeding distributions, the migration speed of cells from population 2 is maintained at 1 μm/hr while cells from population 1 move at speeds of 10 μm/hr (part (a)) and 50 μm/hr (part (b)), respectively.

Cell Population Profiles. Figure 6 shows the cell population profiles of two simulation runs using a segmented wound-seeding distribution and two different values of the ratio R ($R = 1$ and $\frac{1}{9}$, respectively). These profiles are exhibited as 2-D cross sections of the wound area and at different levels of wound coverage. We observe the following:

- At 33% of wound coverage, faster cells cover larger portions of the wound than slow cells as most of the growth appears in the lower partition of both seeding examples. There is also sporadic diffusion of fast cells into the upper partitions.
- At 66% of wound coverage, nearly most of the two lower partitions are covered while the upper partions remain mostly empty. In particular, when $R = \frac{1}{9}$, the lower partition is completely covered whereas the top segment is sparsely occupied by cells when $R = 1$.
- At 99% of wound coverage, the fast cells have penetrated to the top of the cellular space and have completely covered the denuded area at the bottom. Slow cells appear to mostly proliferate toward the center of the wound in a radial direction causing a cone-shaped funneling of the growth of fast cells.

Effect of Cell-Seeding Distributions. Figure 7 shows comparisons between the tissue growth rates obtained by using segmented and mixed distributions in case of wound-seeding mode and with $R = 1$. Cells from population 2 migrate at a fixed speed of 1 μm/hr. In this figure, cells from population 1 have a migration speed of 10 μm/hr in part (a) and 50 μm/hr in part (b), respectively. We observe that the mixed-seeding distribution takes less time to reach confluence and yields higher tissue growth rates. As cell speeds increase, the mixed seeding distribution continues to maintain its advantage resulting in $40 - 50\%$ reduction in the time to reach complete volume coverage, thus healing the wound faster.

6 Conclusion and Future Work

The reported research involved extending a three-dimensional model initially developed by the second author [7]. Our work incorporated the use of a variable number of mammalian cell populations. The simulation results included two populations of cells with different division and migration characteristics. Their effects on the tissue growth rate and population dynamics of cells were elucidated. The research will help speed up progress in the area of tissue engineering where the development of bio-artificial tissues involves extensive and time-consuming experimentation. It also extends the existing features of the model to incorporate others that more realistically simulate the process of tissue growth. Future work involves the parallelization of the model and its implementation on a Beowulf cluster using different decomposition techniques to simulate the growth of realizable tissue objects.

Acknowledgments

We gratefully acknowledge the financial support provided by the Natural Sciences and Engineering Research Council (NSERC) of Canada via a Discovery Grant under project number 31-611407.

References

1. Soll, D., Wessels, D.: Motion analysis of living cells: Techniques in modern biomedical microscopy. Wiley-Liss, New York, NY. (1998)
2. Zygourakis, K., Bizios, R., Markenscoff, P.: Proliferation of anchorage-dependent contact-inhibited cells: I. development of theoretical models based on cellular automata. Biotechnology and Bioengineering **38**(5) (1991) 459–470
3. Zygourakis, K., Markenscoff, P., Bizios, R.: Proliferation of anchorage-dependent contact-inhibited cells. II: Experimental results and validation of the theoretical models. Biotechnology and Bioengineering **38**(5) (1991) 471–479
4. Lee, Y., Markenscoff, P.A., McIntire, L.V., Zygourakis, K.: Characterization of endothelial cell locomotion using a markov chain model. Biochemistry and Cell Biology **73** (1995) 461–472
5. Cherry, R.S., Papoutaskis, E.T.: Modelling of contact-inhibited animal cell growth on flat surfaces and spheres. Biotechnology and Bioengineering **33** (January, 1989) 300–305
6. Lim, J.H.F., Davies, G.A.: A stochastic model to simulate the growth of anchorage dependent cells on flat surfaces. Biotechnology and Bioengineering **36** (September, 1990) 547–562
7. B. Ben Youssef: Simulation of cell population dynamics using 3-D cellular automata. In: Proceedings of the Sixth International Conference on Cellular Automata for Research and Industry (ACRI 2004). Volume 3305., Published by Springer Verlag in Lecture Notes of Computer Science (LNCS) (2004) 562–571
8. B. Ben Youssef, Markenscoff, P., Zygourakis, K.: Parallelization of a 3-D computational model for wound healing. WSEAS Transactions on Computers **3**(4) (2004) 993–998
9. Wolfram, S.: Cellular Automata and Complexity: Collected Papers. Addison-Wesley Publishing Co. (1994)

10. B. Ben Youssef: A three-dimensional stochastic model for tissue growth. In: Proceedings of the 16th IASTED International Conference on Modelling and Simulation (MS 2005). (2005) 136–142
11. Palsson, B.O., Bhatia, S.N.: Tissue engineering. Pearson Prentice Hall, Upper Saddle River, NJ. (2004)
12. Cheng, G., B. Ben Youssef, Markenscoff, P., Zygourakis, K.: Cell population dynamics modulate the rates of tissue growth processes. Biophysical Journal **90**(3) (2006) 713–724